Lawrence Berkeley National Laboratory

Title

Dependence of spin pumping and spin transfer torque upon Ni81Fe19 thickness in Ta/Ag/Ni81Fe19/Ag/Co2MnGe/Ag/Ta spin-valve structures

Permalink

https://escholarship.org/uc/item/8d76d7db

Authors

Durrant, CJ
Shelford, LR
Valkass, RAJ
et al.

Dependence of spin pumping and spin transfer torque upon $Ni_{81}Fe_{19}$ thickness in $Ta/Ag/Ni_{81}Fe_{19}/Ag/Co_2MnGe/Ag/Ta$ spin-valve structures

C. J. Durrant, L. R. Shelford, R. A. J. Valkass, and R. J. Hicken

Department of Physics and Astronomy, University of Exeter, Stocker Road, Exeter, Devon, EX4 4QL, United Kingdom

A. I. Figueroa, A. A. Baker, and G. van der Laan

Magnetic Spectroscopy Group, Diamond Light Source, Didcot, OX11 0DE, United Kingdom

L. B. Duffy

Department of Physics, Clarendon Laboratory, University of Oxford, OX1 3PU, United Kindom

P. Shafer, C. Klewe, and E. Arenholz

Advanced Light Source, Lawrence Berkeley National Laboratory, Berkeley, California 94720, USA

S. A. Cavill

Department of Physics, University of York, YO10 5DD, United Kingdom

J. R. Childress and J. A. Katine

HGST, San Jose, California 95135, USA

Spin pumping has been studied within Ta / Ag / $Ni_{81}Fe_{19}$ (0–5 nm) / Ag (6 nm) / Co_2MnGe (5 nm) / Ag / Ta large-area spin-valve structures, and the transverse spin current absorption of $Ni_{81}Fe_{19}$ sink layers of different thicknesses has been explored. In some circumstances, the spin current absorption can be inferred from the modification of the Co_2MnGe source layer damping in vector network analyzer ferromagnetic resonance (VNA-FMR) experiments. However, the spin current absorption is more accurately determined from element-specific phase-resolved x-ray ferromagnetic resonance (XFMR) measurements that directly probe the spin transfer torque (STT) acting on the sink layer at the source layer resonance. Comparison with a macrospin model allows the real part of the effective spin mixing conductance to be extracted. We find that spin current absorption in the outer Ta layers has a significant impact, while sink layers with thicknesses of less than 0.6 nm are found to be discontinuous and superparamagnetic at room temperature, and lead to a noticeable increase of the source layer damping. For the thickest 5-nm sink layer, increased spin current absorption is found to coincide with a reduction of the zero frequency FMR linewidth that we attribute to improved interface quality. This study shows that the transverse spin current absorption does not follow a universal dependence upon sink layer thickness but instead the structural quality of the sink layer plays a crucial role.

I. INTRODUCTION

The discovery that a spin-polarized current could exert a torque (STT) on a nanoscale ferromagnet (FM) has led to the development of a whole new class of electronic devices [1,2]. Pure spin currents can circumvent the constraints placed on traditional electronics and have the potential to allow low-power and high-bandwidth information transfer [3,4]. Crucial to the development of smaller and more efficient devices is a more complete understanding of the mechanisms by which spin currents can be generated, such as the spin Hall effect [5,6], and how these currents propagate through ultrathin films. Detection of pure spin current has been achieved through measurement of effects induced by the spin current, such as spin-torque driven magnetic precession [7,8] and the inverse spin Hall effect [9–11]. Very recently, methods have been devised to detect the local spin density by means of soft x-ray probes [12].

One mechanism by which the generation and propagation of spin current can be studied is precessional spin pumping. In a spin valve comprising a ferromagnetic/normal/ferromagnetic ($FM_1/NM/FM_2$) metal hybrid structure, magnetic precession in the "source" layer (FM_1) pumps pure spin current into the adjacent non magnetic layer (NM) [13]. A nonlocal damping of FM_1 may then result from spin scattering in the NM. Further damping may occur with the addition of the second ferromagnetic "sink" layer (FM_2) on the opposite interface of the NM. This allows FM_1 to pump spin current across the NM and into FM_2, where the transverse component of the spin current can be absorbed, in a similar manner to the absorption of the spin carried by a charge current [14]. The absorption of the spin current leads to a STT on the sink layer magnetization and increased damping of the precession in the source layer.

Ferromagnetic resonance (FMR) is a powerful technique by which to observe the spin pumping effect [7]. This technique has the advantage that spin current absorption in layers only a few Ångström thick can be measured as a perturbation of the much larger signal from the source layer. This type of measurement does not require nanofabrication and so finite-size magnetostatic effects [15] and activation volume effects

144421-1

[16] do not increase the complexity of the interpretation. However, it does not provide a direct measurement of the spin current absorption in the sink layer.

The spin relaxation length in the NM layer has been studied extensively [17,18]. The penetration of the spin current into the ferromagnetic sink layer has been studied by means of magnetotransport measurements, which have indicated a characteristic length for the absorption of the longitudinal component of spin (i.e., parallel or antiparallel to **M**) in 3d transition metals [19,20]. Here the dependence on distance from the interface z was found to be exponential with spin current density, i.e., $\propto \exp(-z/\lambda_{SD})$, where λ_{SD} is the spin diffusion length. Recently, Ghosh *et al.* [21] used spin pumping to infer that the depth dependence of the transverse component of spin current (i.e., perpendicular to **M**) instead follows a power-law dependence. They found this to be applicable in structurally diverse ferromagnets, with the absorption of the spin current saturating at a FM$_2$ thickness of 1.2 ± 0.1 nm. This result supports theoretical predictions that the length scales are governed by the transverse spin coherence length λ_J which is proportional to $\pi/|k_f^\uparrow - k_f^\downarrow|$ to first order where $k_f^{\uparrow(\downarrow)}$ are the majority (minority) spin state Fermi wave vectors [22].

However, it is not clear how, for real ultrathin layers (<1.2 nm), the structure and magnetic state of the sink layer may affect the spin current absorption. As the layer thickness becomes comparable to the atomic radius, it is highly unlikely that films form as a smooth layer only a few atoms thick. As the film's structural parameters have a significant impact on the magnetic order of the sink layer, the film structure is also expected to have a significant effect on spin current absorption. While other studies focus purely on the sink layer [21], often this layer is part of a larger stack, which adds complexity; i.e., it is not immediately clear what effect this surrounding structure may have on spin absorption. Typically a NM with weak spin-orbit coupling is used in the FM$_1$/NM/FM$_2$ trilayer since, in such materials, the spin-flip rate is comparatively small, meaning that if the thickness of the NM is much smaller than the spin-diffusion length, efficient spin transfer is expected from FM$_1$ to FM$_2$. For example, in this study the maximum NM (Ag) thickness is 6 nm, which is considerably smaller than the spin diffusion length that is estimated to be 158–170 nm [23,24] and it has been demonstrated that Ag is an efficient spacer layer for the injection of spin current [19,25]. When other NM layers are present in the layered structure, their effect must also be considered, especially if they contain heavy elements with large spin-orbit coupling.

Since the spin current can be eliminated by spin-flip scattering at the FM/NM interfaces [26] and within the NM layers, it is critical to directly observe the response of the sink layer, in conjunction with the source, in order to unambiguously conclude that spin absorption within the sink layer is responsible for an increased damping of the source layer. The dynamics of the sink layer have previously been observed by time-resolved magneto-optical Kerr effect studies [23,27,28] of epitaxial structures with Ag and Au spacer layers. In spin valves with chemically distinct source and sink layers, the element selectivity of x-ray magnetic circular dichroism (XMCD) [29] can be employed to isolate the dynamic response of the source and sink layers and directly probe the spin torque acting on the sink layer.

In this study, vector network analyzer ferromagnetic resonance (VNA-FMR) is used to determine the dependence of the source layer damping parameter α (which not only has the well-established Gilbert damping contribution, but also an additional contribution caused by absorption of the spin current in FM$_2$) as a function of the sink layer thickness (t_{NiFe}). The value of (t_{NiFe}) is varied from 0 to 5 nm so as to fully explore the length scales for absorption of the transverse component of spin current. X-ray-detected ferromagnetic resonance (XFMR) is used to make layer-selective measurements of the amplitude and phase of precession in the source and sink layers. XFMR measurements are required to determine unambiguously whether spin angular momentum taken from the source layer is absorbed by the sink layer or lost elsewhere in the sample stack. By probing the torque acting on the sink layer in the experiment, the real part of the effective spin mixing conductance $\mathrm{Re}(g_{\mathrm{eff}}^{\uparrow\downarrow})$ may be deduced.

II. EXPERIMENTAL

Each spin valve structure was deposited on a sapphire wafer onto which a Ta (5 nm) / Cu (100 nm) / Ta (5 nm) / Ru (10 nm) overlayer had previously been deposited by magnetron sputtering. A 60-s rf etch was used to remove 3.5 nm of Ru, ensuring a clean surface, before magnetron sputtering was again used to deposit spin valve stacks in the order Ta (5 nm) / Ag (4 nm) / Ni$_{81}$Fe$_{19}$ (0.3–5.0 nm) / Ag (6 nm) / Co$_2$MnGe (5 nm) / Ag (2 nm) / Ta (3 nm). Control samples, one without the Ni$_{81}$Fe$_{19}$ layer comprising Ta (5 nm) / Ag (6 nm) / Co$_2$MnGe (5 nm) / Ag (2. nm) / Ta (3 nm), and a second without the Co$_2$MnGe layer comprising Ta (5 nm) / Ag (4 nm) / Ni$_{81}$Fe$_{19}$ (3 nm) / Ag (6 nm) / Ta (3 nm) were also fabricated. In the as-deposited state, the Co$_2$MnGe source layer is nonmagnetic due to disorder. Field annealing is used to induce the ordered ferromagnetic state and induces a small (<10 Oe) in-plane uniaxial magnetic anisotropy within both layers. VNA-FMR and XFMR measurements were performed on large-area 1×1 cm^2 films.

VNA-FMR measurements were made by placing samples face down on a 50 Ω coplanar waveguide (CPW) with 500-μm signal track width [Fig. 1(a)]. A 100-nm layer of photoresist was used to prevent the sample from short circuiting the CPW. The scattering matrix parameters of the composite structure were recorded for frequencies from 0 to 15 GHz as the bias field was swept between 0.0 and 1.3 kOe [30]. The damping parameter (α) of FM$_1$ (Co$_2$MnGe) was extracted from the frequency-dependent full width half maximum linewidths
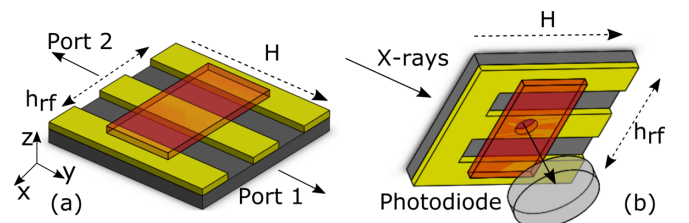

FIG. 1. (a) Measurement geometries for vector network analyser ferromagnetic resonance (VNA-FMR) and (b) x-ray detected ferromagnetic resonance (XFMR).

$\Delta H(\omega)$ for each FM$_2$ (Ni$_{81}$Fe$_{19}$) thickness using [31]

$$\Delta H(\omega) = \Delta H(0) + 2\alpha\omega/\gamma, \qquad (1)$$

where $\Delta H(0)$ is the contribution due to inhomogeneous broadening.

Phase-resolved XFMR measurements [12,32,33] were made upon the same continuous thin films. The sample was placed in contact with a coplanar waveguide fabricated from a printed circuit board. A countersunk hole of 500-μm diameter in the 1-mm-wide signal line allowed x-ray access to the sample. Circularly polarized x rays were used to determine the magnetization along the beam direction. The transmitted x rays were detected indirectly through x-ray excited optical luminescence in the sapphire substrate, with the emitted light detected by a photodiode mounted behind the sample [Fig. 1(b)]. An in vacuum SMA cable was used to deliver a 4-GHz rf current to the CPW, generating an in-plane oscillating magnetic field at the sample surface, exciting precession. A comb generator driven by the 499.65-MHz synchrotron master clock ensured phase coherence of higher harmonics with the x-ray bunches. A static bias field, applied parallel to the CPW signal line, was swept to reveal the ferromagnetic resonance. This transverse geometry allows phase-resolved measurement of the precession by delaying the rf excitation relative to the synchrotron master clock signal using a delay line with a resolution of 2 ps. Layer specificity was achieved by tuning the x-ray energy to either the Co L_3 edge in the source (Co$_2$MnGe) layer or the Fe L_3 edge in the sink (Ni$_{81}$Fe$_{19}$) layer, allowing direct measurement of the spin dynamics in each layer.

III. RESULTS

A. Vector network analyzer ferromagnetic resonance (VNA-FMR) measurements

Typical VNA-FMR resonance spectra acquired at a frequency of 8 GHz for different sink layer thicknesses (t_{NiFe}) are shown in Fig. 2. For $t_{NiFe} = 1.2$ (b) and 1.8 nm (c) both the Co$_2$MnGe and Ni$_{81}$Fe$_{19}$ peaks are distinct and visible, allowing observation of the sink layer resonance directly. For $t_{NiFe} \leqslant 0.9$ nm, as in Fig. 2(a), the Ni$_{81}$Fe$_{19}$ resonance cannot be identified unambiguously and therefore using this technique, information about the behavior of the sink layer can only be inferred from the dynamics of the source layer.
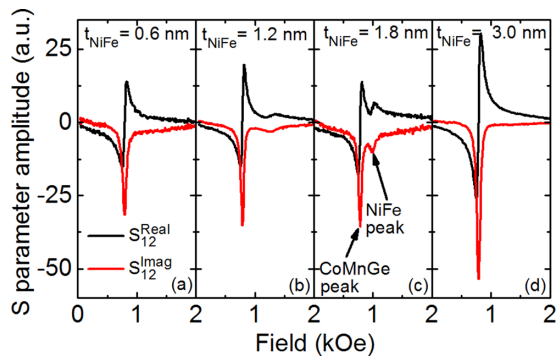

FIG. 2. Typical experimental VNA-FMR field sweeps at $f = 8$ GHz for sink layer thicknesses of (a) $t_{NiFe} = 0.6$, (b) 1.2, (c) 1.8, and (d) 3.0 nm, showing the S_{12}^{Im} and S_{12}^{Re} scattering matrix components.
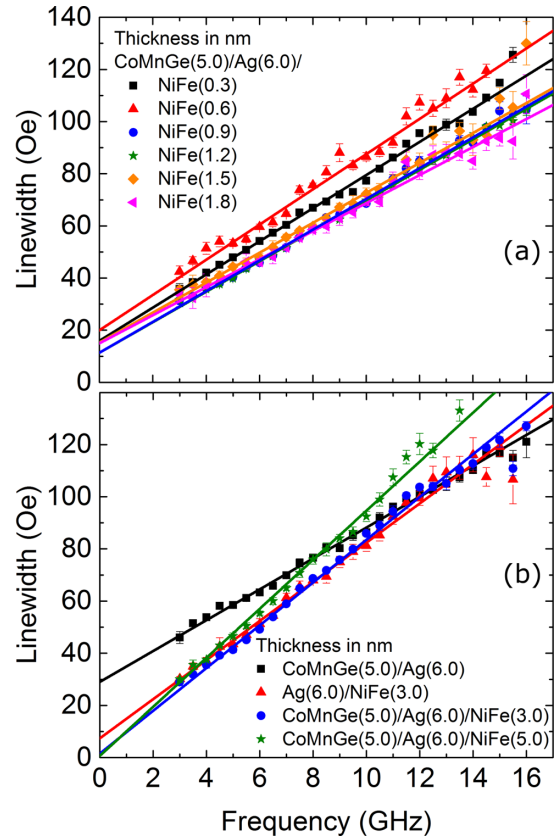

FIG. 3. VNA-FMR measurements showing frequency-dependent Co$_2$MnGe linewidths and linear fits to (a) the thick sink layer [Co$_2$MnGe (5 nm) / Ag (6 nm) / Ni$_{81}$Fe$_{19}$ (3.0–5.0 nm)] trilayers, along with single-layer reference films without the source layer [Ag (6 nm) / Ni$_{81}$Fe$_{19}$ (3.0 nm)] and without the sink layer [Co$_2$MnGe (5 nm) / Ag (6 nm)], and (b) thin sink layer [Co$_2$MnGe (5 nm) / Ag (6 nm) / Ni$_{81}$Fe$_{19}$ (0.3–1.8 nm)] trilayers. These plots are separated for clarity.

For the thickest films in this study, $t_{NiFe} = 3.0$ [Fig. 2(d)] and 5.0 nm, the Co$_2$MnGe and Ni$_{81}$Fe$_{19}$ peaks overlap, making it impossible to resolve the behavior of the individual layers.

For each sample, the damping parameter of the source layer has been extracted from the frequency-dependent linewidth $\Delta H(\omega)$ [as in Eq. (1)] obtained by fitting a single Lorentzian function to the absorptive (S_{12}^{Im}) S parameter. The intrinsic damping has been isolated as in Ref. [31]. Figure 3(a) shows linewidth versus frequency for the two single-layer reference samples. Here $\Delta H(0)$ is comparatively large for the Co$_2$MnGe single layer and small for the Ni$_{81}$Fe$_{19}$ single layer. The measured line widths for the trilayer stacks with $t_{NiFe} = 0.3$–1.8 nm are shown in Fig. 3(b). Figure 4(a) shows that the general trend is for $\Delta H(0)$ to decrease with increasing Ni$_{81}$Fe$_{19}$ thickness. For $t_{NiFe} = 3.0$–5.0 nm, $\Delta H(0)$ is negligible. As $\Delta H(0)$ usually results from structural imperfections [34], and the Co$_2$MnGe layer is grown after the Ni$_{81}$Fe$_{19}$ layer, this result suggests that the increased Ni$_{81}$Fe$_{19}$ thickness enhances the quality of the Co$_2$MnGe growth. The insight gained from VNA-FMR about $\Delta H(0)$ is crucial for the fitting and interpretation of the more complex XFMR experiment discussed further below.
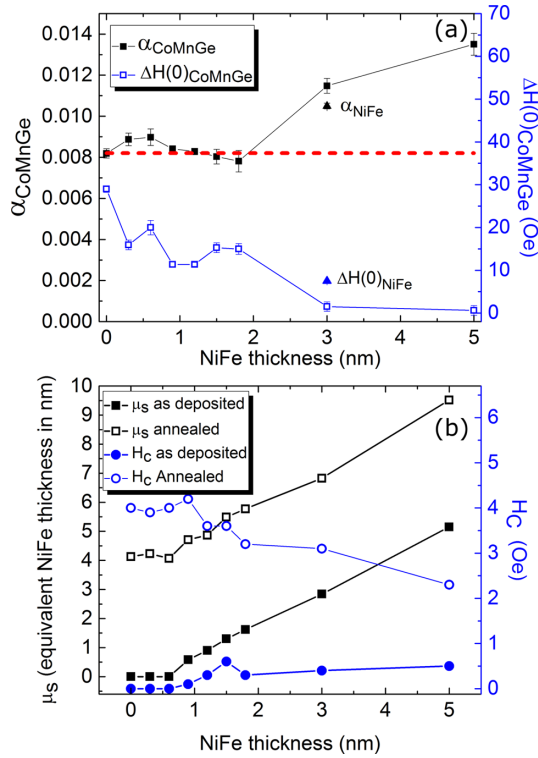
FIG. 4. (a) Gilbert damping parameter, α, and inhomogeneous broadening $\Delta H(0)$ of Co_2MnGe measured by vector network analyzer ferromagnetic resonance (VNA-FMR) (the dashed red line is a guide to the eye) and (b) saturation moment per unit area μ_S (given in units of equivalent $Ni_{81}Fe_{19}$ thickness, assuming saturation magnetization M_s for $Ni_{81}Fe_{19} \approx 860$ emu/cm^3) [38], and coercive field (H_c) measured by vibrating sample magnetometry (VSM) as a function of $Ni_{81}Fe_{19}$ layer thickness in $Co_2MnGe/Ag/Ni_{81}Fe_{19}$ spin valve structures. All measurements, in both panels (a) and (b), were performed at 300 K.

Figure 4(a) shows α_{CoMnGe} for each $Ni_{81}Fe_{19}$ sink layer thickness. Error bars in this figure represent the statistical error associated with the fit. For $t_{NiFe} \leqslant 1.8$ nm, the variation of α_{CoMnGe} is relatively small. In this region, the only samples that show a significantly different value of the damping parameter are $t_{NiFe} = 0.3$ and 0.6 nm. At first sight, this is surprising since other studies have reported a power law increase in α_{source} with sink layer thickness [21]. The relative insensitivity to t_{NiFe} might lie in the presence of the Ta layer adjacent to the sink. Ta has a large atomic number, and hence large spin-orbit coupling, and therefore scatters injected spins effectively. As a consequence, a spin current that passes through the thin $Ni_{81}Fe_{19}$ layer then also passes across the adjacent Ag layer and is strongly scattered within the Ta.

The increase in damping for the thinnest $Ni_{81}Fe_{19}$ thicknesses, $t_{NiFe} = 0.3$ and 0.6 nm, may be due to the atomic scale structure of the $Ni_{81}Fe_{19}$ layer. Magnetic hysteresis loops acquired by vibrating sample magnetometry (VSM) are presented within the Supplementary Material [35]. The saturation moment per unit area plotted in Fig. 4(b) shows that for $t_{NiFe} \leqslant 0.6$ nm the $Ni_{81}Fe_{19}$ layer does not exhibit ferromagnetic order. Since Fe and Ni are known to be immiscible in Ag [36], intermixing and alloy formation with

the adjacent Ag layers can be ruled out. $Ni_{81}Fe_{19}$ films on Ag are found to have a lattice parameter of 0.36 nm [37]. When the layer thickness is comparable to the lattice parameter, it is highly unlikely that a continuous single layer film is formed. Furthermore, AFM measurements [2] have shown that sputter deposition of Ag on to a Ta underlayer results in a surface roughness of order 1 nm. Therefore, it is likely that the $Ni_{81}Fe_{19}$ layers are discontinuous, with the grains being superparamagnetic at room temperature, and that the greater structural and magnetic disorder leads to increased spin scattering. Figure 4(b) demonstrates that the ferromagnetic Co_2MnGe state is induced by field annealing.

Finally, the extracted α_{CoMnGe} values for the thickest $Ni_{81}Fe_{19}$ layers $t_{NiFe} = 3.0$ and $t_{NiFe} = 5.0$ nm appear to rise sharply. However, the Co_2MnGe and $Ni_{81}Fe_{19}$ resonances overlap closely in the frequency and field range considered here [Fig. 2(d)] to the extent that separate resonances could not be observed in the VNA-FMR experiment. The increase in α could therefore arise from a small but finite difference between the Co_2MnGe and $Ni_{81}Fe_{19}$ resonance fields. Therefore, the extracted values provide an upper limit for α_{CoMnGe} and the response of the two ferromagnetic layers needs to be separated before any further conclusions can be drawn.

B. X-ray ferromagnetic resonance (XFMR) measurements

XFMR field scans at $h_{rf} = 4$ GHz are shown in Fig. 5. The solid lines are the result of numerical modeling that will be described below. The dispersive (Re) and absorptive (Im) components of the signal are initially mixed due to a phase delay present within the microwave electronics of the measurement apparatus. These components are recovered by rotating the complex signal in the Argand plane so as to obtain maximum peak height in the Im component at the position of maximum gradient in the Re component, and a flat response on either side of the resonance. For both $t_{NiFe} = 1.5$ nm [Fig. 5(a)] and 1.8 nm [Fig. 5(b)], the Co Im and Fe Re data show a clear peak at the Co_2MnGe resonance field $H_{res} = 204$ Oe, while the Fe Im signal shows a peak at the thickness dependent $Ni_{81}Fe_{19}$ resonance fields of $H_{res} = 303$ and 258 Oe, respectively. Crucially it is possible to observe the response of the $Ni_{81}Fe_{19}$ sink layer at the Co_2MnGe source layer resonance field (204 Oe). At resonance, the Im part of the Co_2MnGe response is unipolar while, at the same field, the Im part of the $Ni_{81}Fe_{19}$ response is bipolar (a negative peak followed by a positive peak). This behavior is reversed for the Re part of the Co_2MnGe response. This is a distinct signature of STT due to spin pumping (rather than static dipolar or exchange coupling) and corresponds to a bipolar variation of the sink layer phase at the source layer resonance [32]. For the thicker $t_{NiFe} = 3.0$ and 5.0 nm films, the resonances of the two magnetic films overlap and the manifestation of spin pumping is an asymmetry of the line shape. This can be seen most clearly for the $t_{NiFe} = 5.0$ nm film where the Co_2MnGe line shape shows a difference in height and shape of the lobes in the Re component and a difference in gradient between the low- and high-field sloping regions of the Im component. Both effects are predicted and described well by numerical modeling, as described below.
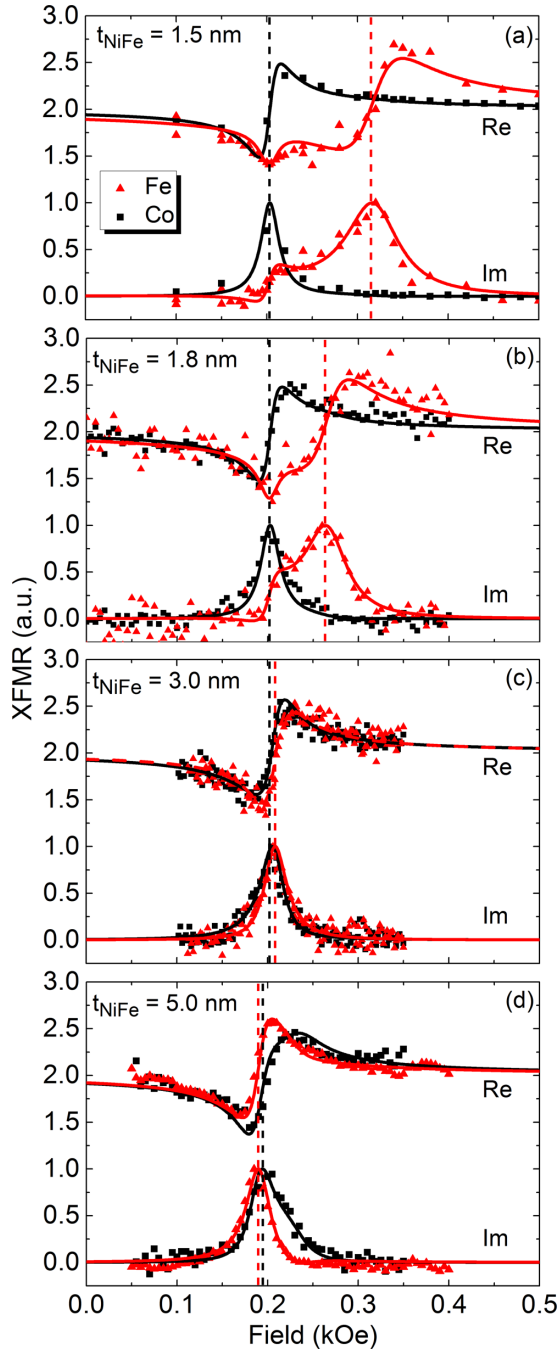
FIG. 5. The Re and Im components of layer specific XFMR field scans at 4 GHz, for Co_2MnGe (5.0 nm) / Ag (6 nm) / $Ni_{81}Fe_{19}$ [1.5 (a), 1.8 (b), 3.0 (c), and 5.0 (d) nm]. The solid lines were obtained from numerical simulations in which Eqs. (2) and (5) were solved simultaneously. The dashed vertical lines highlight the resonant fields of the Co_2MnGe (black) and $Ni_{81}Fe_{19}$ (red) layers.

The dynamic behavior can be modeled using coupled LLG equations, with additional terms to describe the spin pumping [7,32]. The precessing magnetization of each layer has two oscillatory (transverse) dynamic components. Since the XMCD arises from the magnetization component parallel to the x-ray wave vector, the x rays sample the projection of the transverse components along the beam direction. The LLG

equation for the response of the ith layer including the effects of interactions with the jth layer can be written as

$$\frac{\partial \mathbf{m}_i}{\partial t} = -|\gamma| \mathbf{m}_i \times \left[\mathbf{H}_{\text{eff}}^i + \beta_i \mathbf{M}_j - \frac{\alpha_i^{(0)} + \alpha_{ii}'}{|\gamma_i|} \frac{\partial \mathbf{m}_i}{dt} \right]$$
$$- \alpha_{ij}' \mathbf{m}_j \times \frac{\partial \mathbf{m}_j}{\partial t}, \tag{2}$$

where $\mathbf{m}_i$ and $\mathbf{m}_j$ are unit vectors parallel to the magnetization vectors of the ith and jth layers. There are four torque terms represented in Eq. (2). The first term gives the torque due to the local effective field $\mathbf{H}_{\text{eff}}^i$ including applied field, crystalline anisotropy, and shape anisotropy. The second term gives the torque arising from dipolar or indirect exchange interactions with the other layer. The third term gives the effective Gilbert type damping, including both intrinsic spin-orbit effects and two magnon scattering, and an extra term in α_{ii}' due to spin pumping with layer i as the source. The final torque term arises due to spin pumping from the other layer j, with layer i as the sink. In the following analysis, the Co_2MnGe layer is denoted by the subscript 1, and the $Ni_{81}Fe_{19}$ layer is denoted by the subscript 2.

For the present samples, the second and fourth terms (coupling and spin pumping from other layer) are relatively weak. Therefore, to lowest order, the position of the resonance for a particular layer can be described by the solution of the LLG equation for that layer, when it is isolated from the other. The magnetocrystalline anisotropy field is small and so the in-plane uniaxial anisotropy is neglected. The layer is sufficiently thin so that surface anisotropy associated with the interfaces may have a significant effect. This contribution is combined with the shape anisotropy to generate a single perpendicular anisotropy field for each magnetic layer. With these assumptions, the relation between field and frequency at resonance can be written as

$$\omega_r^2 = \gamma^2 H_{\text{res}}(H_{\text{res}} + 4\pi M_{\text{eff}}), \tag{3}$$

where ω_r is the resonance frequency, H_{res} is the resonance field, $\gamma = \gamma_e g / 2$ where $\gamma_e = 2\pi(2.80)$ MHz/Oe, and the spectroscopic splitting factor g is assumed to be 2.11 for $Ni_{81}Fe_{19}$ [39] and 2.00 for Co_2MnGe [40]. The effective demagnetizing field $4\pi M_{\text{eff}} = 4\pi M - 4K_s / Mt$, where K_s is the surface anisotropy constant, which is assumed to have the same value for both surfaces of the layer. For a given film thickness t, the saturation magnetization M is found from the VSM data [Fig. 4(b)]. The value of K_s is then adjusted to obtain the experimental value of ω_r. The spin pumping contribution to the Gilbert damping coefficient has the form [24,32]

$$\alpha_{ij}' = \frac{g_i \mu_B \text{Re}(g_j^{\uparrow\downarrow})}{8\pi M_i t_i}, \tag{4}$$

where $\text{Re}(g^{\uparrow\downarrow})$ is the Real part of the spin mixing conductance. This form assumes scrambling of the distribution function at the interfaces [7] but is not corrected for the Sharvin conductance [24,41]. The simplifying approximation that $g_1^{\uparrow\downarrow} = g_2^{\uparrow\downarrow} = g^{\uparrow\downarrow}$ is made so that $\alpha_{11}' = \alpha_{12}' = \alpha_1'$ and $\alpha_{22}' = \alpha_{21}' = \alpha_2'$ with

$$\alpha_1' = \frac{g_1 M_2 t_2}{g_2 M_1 t_1} \alpha_2'. \tag{5}$$

TABLE I. Damping parameters (α_1^0, α_1', α_2^0, and α_2'), extracted from the fits to XFMR data shown in Fig. 5, and $\mathrm{Re}(g_{\mathrm{eff}}^{\uparrow\downarrow})$ calculated from Eq. (4) for spin valves with increasing sink layer thickness (t_{NiFe}). † indicates an estimation of the uncertainty in $\mathrm{Re}(g_{\mathrm{eff}}^{\uparrow\downarrow})$ for $t_{\mathrm{NiFe}} = 3.0$ nm which is difficult because the resonance fields of the Co_2MnGe and $Ni_{81}Fe_{19}$ layers are almost identical, which leads to a level of degeneracy in the fitting (see Supplementary Material [35]).

t_{NiFe} (nm)	α_1^0 $\times 10^{-3}$	α_1' $\times 10^{-3}$	α_2^0 $\times 10^{-3}$	α_2' $\times 10^{-3}$	$\mathrm{Re}(g_{\mathrm{eff}}^{\uparrow\downarrow})$ $\times 10^{15}$ (cm^{-2})
1.5	8.2	5.2	5.3	19.0	2.52±0.3
1.8	8.4	4.6	7.1	14.3	2.22 ±0.2
3.0	8.7	9.1	11.0	8.4	2.65 †
5.0	8.7	16.0	9.9	14.0	7.73±2.4

The XFMR data was fitted by means of a least squares regression algorithm. In each case, the layer magnetization M_i was set to the value measured by VSM, shown in Fig. 4(b). The surface anisotropy constant for Co_2MnGe was constrained to $K_{s1} = -0.090$ erg cm^{-2}. The surface anisotropy constant for $Ni_{81}Fe_{19}$ had the fitted values $K_{s2} = 0.085$, 0.088, 0.120, and 0.086 erg cm^{-2} for $t_{\mathrm{NiFe}} = 1.5$, 1.8, 3.0, and 5.0 nm respectively. For $t_{\mathrm{NiFe}} = 1.5$ and 1.8 nm α_1' and α_1^0 were fixed in the relation $\alpha_1^T = \alpha_1' + \alpha_1^0$ where α_1^T is an effective value that also accounts for the line-width offset at zero frequency $\Delta H(0)$, and is derived from the VNA-FMR measured linewidth at 4 GHz shown in Fig. 3(b). This is appropriate for the $t_{\mathrm{NiFe}} = 1.5$ and 1.8 nm trilayer films where the Co_2MnGe and $Ni_{81}Fe_{19}$ resonances are distinct and α_1^T can be extracted directly from the VNA-FMR data. However, for the $t_{\mathrm{NiFe}} = 3.0$ and 5.0 nm trilayer films, the Co_2MnGe and $Ni_{81}Fe_{19}$ resonances are overlapped in the VNA-FMR measurement so direct extraction of α_1^T is not possible. Instead, for $t_{\mathrm{NiFe}} = 3.0$ and 5.0 nm, α_1^0 is fixed using the VNA-FMR measurement of the Co_2MnGe (5.0 nm) reference film (no $Ni_{81}Fe_{19}$ layer) shown in Fig. 3(b). It can be seen in Fig. 3 that growth on $Ni_{81}Fe_{19}$ reduces $\Delta H(0)$. For the $t_{\mathrm{CoMnGe}} = 5.0$ nm reference film $\Delta H(0) = 29$ Oe, and for the trilayer films with $t_{\mathrm{NiFe}} = 3.0$–5.0 nm, $\Delta H(0)$ is reduced to 0 Oe. This is taken into account in the fits and the α_1^0 parameter, which is fixed in the fitting of trilayer films, is calculated from the reference film linewidth minus $\Delta H(0)$. When fitting the $t_{\mathrm{NiFe}} = 3.0$ nm trilayer film α_2^0 was also fixed at the value extracted from VNA-FMR measurements on the $t_{\mathrm{NiFe}} = 3.0$ nm reference film (no Co_2MnGe layer). For all films the relative size of α_1' and α_2' is constrained by Eq. (5).

The fits are shown in Fig. 5 and describe both the source and sink layer resonances well. Inserting the fitted parameter α_2' into Eq. (4) then yields an effective spin mixing conductance for the multilayer structure, $\mathrm{Re}(g_{\mathrm{eff}}^{\uparrow\downarrow})$, for each $Ni_{81}Fe_{19}$ thickness. The values of the α parameters and $\mathrm{Re}(g_{\mathrm{eff}}^{\uparrow\downarrow})$ are listed in Table I. The α_1^0 parameter for the trilayer $t_{\mathrm{NiFe}} = 1.5$-, 1.8-nm films is seen to agree closely with the α_1^0 of the reference Co_2MnGe film measured by VNA-FMR (used to fit the $t_{\mathrm{NiFe}} = 3.0$-, 5.0-nm films). The uncertainty in $\mathrm{Re}(g_{\mathrm{eff}}^{\uparrow\downarrow})$ is, however, particularly large for $t_{\mathrm{NiFe}} = 3.0$ nm because the resonance fields of the Co_2MnGe and $Ni_{81}Fe_{19}$ layers are almost identical, as is evident from Fig. 5(c). In

this case, the two magnetizations precess with close to the same phase and so the two spin pumping terms in Eq. (1) almost cancel, as noted previously by Heinrich *et al.* [7], so that the fitting is less sensitive to the magnitude of their prefactors. A particularly large value for $\mathrm{Re}(g_{\mathrm{eff}}^{\uparrow\downarrow})$ is observed for the $t_{\mathrm{NiFe}} = 5.0$-nm trilayer, where the spin-pumping effect manifests as a pronounced asymmetry of the Co_2MnGe signal that is not present for the other t_{NiFe} values. The sensitivity of each fitted curve to the spin pumping was explored by generating a family of curves around the curve that minimised the sum of the residuals, as shown in the Supplementary Material [35]. The confidence intervals for the $\mathrm{Re}(g_{\mathrm{eff}}^{\uparrow\downarrow})$ values in Table I correspond to the curves for which the fit to the data was visibly worse.

The value of $\mathrm{Re}(g_{\mathrm{eff}}^{\uparrow\downarrow})$ is a measure of the spin-pumping efficiency and is related to the number of conducting channels per spin [41]. An approximate expression for this quantity is given by [24] $\mathrm{Re}(g^{\uparrow\downarrow}) \approx 1.2n^{2/3}$, where n is the density of electrons per spin in the NM. For the projected area of a spherical Ag Fermi surface, $\mathrm{Re}(g^{\ddagger\downarrow}) \approx 1.80 \times 10^{15}$ cm^{-2}. Improved agreement can be expected following correction for the Sharvin conductance [24]; however, this requires *ab initio* electronic structure calculations. A full description should also include separate values of $g^{\uparrow\downarrow}$ for each interface at which spin scattering can be expected to occur. Therefore, the values stated here can be regarded as effective values that describe the two dissimilar interfaces and any internal structure of the spacer layer.

The values of $\mathrm{Re}(g_{\mathrm{eff}}^{\uparrow\downarrow})$ shown in Table 1 for $t_{\mathrm{NiFe}} = 1.5$, 1.8, and 3.0 nm are in reasonable agreement with those expected for a Ag spacer layer with a spherical Fermi surface. The large increase in $\mathrm{Re}(g_{\mathrm{eff}}^{\uparrow\downarrow})$ for $t_{\mathrm{NiFe}} = 5.0$ nm is unexpected in light of the work of Ghosh *et al.* [21]. Given that the $\Delta H(0)$ decreases simultaneously, it seems most likely that the increase in $\mathrm{Re}(g_{\mathrm{eff}}^{\uparrow\downarrow})$ results from improved interface quality at the upper surface of the $Ni_{81}Fe_{19}$ layers that in turns leads to a smoother Co_2MnGe layer. The rather large value of $\mathrm{Re}(g_{\mathrm{eff}}^{\uparrow\downarrow})$ observed for $t_{\mathrm{NiFe}} = 5.0$ nm suggests that either the detailed shape of the Ag Fermi surface needs to be accounted for more carefully, or perhaps that the theoretical description of spin pumping is incomplete for the case of overlapping resonances where spins are pumped from both ferromagnetic layers.

IV. SUMMARY

Spin pumping has been studied in Co_2MnGe/Ag/$Ni_{81}Fe_{19}$ spin valves with varying sink layer thickness. Using VNA-FMR the transverse spin current absorption in the sink layer was inferred from the source layer damping parameter. Unlike previous studies, which have shown a power-law decay, little variation of the spin current absorption was observed over the 0- to 1.8-nm thickness range, a behavior attributed to additional spin scattering in the surrounding stack structure. Small deviations in spin absorption are seen for the thinnest $Ni_{81}Fe_{19}$ layers and are associated with the structural disorder and consequent superparamagnetism of the sink layer for $t_{\mathrm{NiFe}} \leqslant 0.6$ nm. The VNA-FMR experiment highlights the complexities and potential pitfalls of indirect observation of

spin pumping and the need for careful consideration and categorization of each layer in the stack.

Phase-resolved XFMR measurements were used to directly probe the torque on the sink layer and revealed a characteristic bipolar phase behavior of the sink layer at the source layer resonance, a clear fingerprint of spin-current-driven precession. The observed behavior is reproduced well by a macrospin model that allows the real part of the spin mixing conductance to be determined. However, when the source and sink layer resonances are coincident, there is a cancellation of the spin currents pumped from the two ferromagnetic layers and the XFMR experiment becomes relatively insensitive to the value of the effective spin mixing conductance $\text{Re}(g_{\text{eff}}^{\uparrow\downarrow})$. For the samples with the thickest (5-nm) $\text{Ni}_{81}\text{Fe}_{19}$ layer, an increased value of $\text{Re}(g_{\text{eff}}^{\uparrow\downarrow})$ is observed simultaneously with a reduction of $\Delta H(0)$, suggesting that both changes are a consequence of improved interface quality.

In conclusion, we have shown that measurements of the source layer linewidth within a spin valve do not always provide the means to fully determine the spin mixing conductance due to spin current absorption in capping and buffer layers in a multilayer stack. Instead, XFMR can be used to determine the effective spin mixing conductance $\text{Re}(g_{\text{eff}}^{\uparrow\downarrow})$ from the spin transfer torque exerted upon the sink layer. Our measurements show that the thickness-dependent structural quality of the stack has a significant influence upon the extracted $\text{Re}(g_{\text{eff}}^{\uparrow\downarrow})$ values.

[1] E. Y. Tsymbal and I. Žutić, *Handbook of Spin Transport and Magnetism* (CRC Press, Boca Raton, FL, 2012).

[2] S. H. Park, K. S. Lee, and A. S. Reddy, Low emissivity Ag/Ta/glass multilayer thin films deposited by sputtering, J. Appl. Phys. **110**, 063508 (2011).

[3] I. Žutić and H. Dery, Spintronics: Taming spin currents, Nat. Mat. **10**, 647 (2011).

[4] T. Yang, T. Kimura, and Y. Otani, Giant spin-accumulation signal and pure spin-current-induced reversible magnetization switching, Nat. Phys. **4**, 851 (2008).

[5] J. Sinova, S. O. Valenzuela, J. Wunderlich, C. H. Back, and T. Jungwirth, Spin Hall effects, Rev. Mod. Phys. **87**, 1213 (2015).

[6] Y. K. Kato, R. C. Myers, A. C. Gossard, and D. D. Awschalom, Observation of the spin Hall effect in semiconductors, Science **306**, 1910 (2004).

[7] B. Heinrich, Y. Tserkovnyak, G. Woltersdorf, A. Brataas, R. Urban, and G. E. W. Bauer, Dynamic Exchange Coupling in Magnetic Bilayers, Phys. Rev. Lett. **90**, 187601 (2003).

[8] S. I. Kiselev, J. C. Sankey, I. N. Krivorotov, N. C. Emley, R. J. Schoelkopf, R. A. Buhrman, and D. C. Ralph, Microwave oscillations of a nanomagnet driven by a spin-polarized current, Nature (London) **425**, 380 (2003).

[9] M. V. Costache, M. Sladkov, S. M. Watts, C. H. van der Wal, and B. J. van Wees, Electrical Detection of Spin Pumping Due to the Precessing Magnetization of a Single Ferromagnet, Phys. Rev. Lett. **97**, 216603 (2006).

[10] T. Kimura, Y. Otani, T. Sato, S. Takahashi, and S. Maekawa, Room-Temperature Reversible Spin Hall Effect, Phys. Rev. Lett. **98**, 156601 (2007).

[11] E. Saitoh, M. Ueda, H. Miyajima, and G. Tatara, Conversion of spin current into charge current at room temperature: Inverse spin-Hall effect, Appl. Phys. Lett. **88**, 182509 (2006).

[12] J. Li, L. R. Shelford, P. Shafer, A. Tan, J. X. Deng, P. S. Keatley, C. Hwang, E. Arenholz, G. Van Der Laan, R. J. Hicken, and Z. Q. Qiu, Direct Detection of Pure ac Spin Current by X-Ray Pump-Probe Measurements, Phys. Rev. Lett. **117**, 076602 (2016).

[13] Y. Tserkovnyak, A. Brataas, and G. E. W. Bauer, Enhanced Gilbert Damping in Thin Ferromagnetic Films, Phys. Rev. Lett. **88**, 117601 (2002).

[14] D. Wei, M. Obstbaum, M. Ribow, C. H. Back, and G. Woltersdorf, Spin Hall voltages from a.c. and d.c. spin currents, Nat. Commun. **5**, 3768 (2014).

[15] R. D. McMichael and M. D. Stiles, Magnetic normal modes of nanoelements, J. Appl. Phys. **97**, 10J901 (2005).

[16] P. Krone, D. Makarov, M. Albrecht, T. Schrefl, and D. Suess, Magnetization reversal processes of single nanomagnets and their energy barrier, J. Mag. Mag. Mat. **322**, 3771 (2010).

[17] Th. Gerrits, M. L. Schneider, and T. J. Silva, Enhanced ferromagnetic damping in Permalloy/Cu bilayers, J. Appl. Phys. **99**, 023901 (2006).

[18] X. Lou, C. Adelmann, S. A. Crooker, E. S. Garlid, J. Zhang, K. S. M. Reddy, S. D. Flexner, C. J. Palmstrøm, and P. A. Crowell, Electrical detection of spin transport in lateral ferromagnet-semiconductor devices, Nat. Phys. **3**, 197 (2007).

[19] J. Bass and W. P. Pratt, Spin-diffusion lengths in metals and alloys, and spin-flipping at metal/metal interfaces: An experimentalist's critical review, J. Phys.: Condens. Matter **19**, 183201 (2007).

[20] Q. Yang, P. Holody, S.-F. Lee, L. L. Henry, R. Loloee, P. A. Schroeder, W. P. Pratt, and J. Bass, Spin Flip Diffusion Length and Giant Magnetoresistance at Low Temperatures, Phys. Rev. Lett. **72**, 3274 (1994).

[21] A. Ghosh, S. Auffret, U. Ebels, and W. E. Bailey, Penetration Depth of Transverse Spin Current in Ultrathin Ferromagnets, Phys. Rev. Lett. **109**, 127202 (2012).

[22] J. Zhang, P. M. Levy, S. Zhang, and V. Antropov, Identification of Transverse Spin Currents in Noncollinear Magnetic Structures, Phys. Rev. Lett. **93**, 256602 (2004).

[23] B. Kardasz, O. Mosendz, B. Heinrich, Z. Liu, and M. Freeman, Spin current studies in Fe/Ag, Au/Fe by ferromagnetic resonance and time-resolved magneto-optics, J. Appl. Phys. **103**, 07C509 (2008).

[24] B. Kardasz and B. Heinrich, Ferromagnetic resonance studies of accumulation and diffusion of spin momentum density in Fe/Ag/Fe/GaAs(001) and Ag/Fe/GaAs(001) structures, Phys. Rev. B. **81**, 094409 (2010).

[25] J. C. Rojás Sanchez, L. Vila, G. Desfonds, S. Gambarelli, J. P. Attané, J. M. De Teresa, C. Magén, and A. Fert, Spin-to-charge conversion using Rashba coupling at the interface between nonmagnetic materials, Nat. Commun. **4**, 2944 (2013).

[26] J. C. Rojás Sanchez, N. Reyren, P. Laczkowski, W. Savero, J. P. Attané, C. Deranlot, M. Jamet, J.-M. George, L. Vila, and H. Jaffrés, Spin Pumping and Inverse Spin Hall Effect in Platinum: The Essential Role of Spin-Memory Loss at Metallic Interfaces, Phys. Rev. Lett. **112**, 106602 (2014).

[27] O. Mosendz, G. Woltersdorf, B. Kardasz, B. Heinrich, and C. H. Back, Magnetization dynamics in the presence of pure spin currents in magnetic single and double layers in spin ballistic and diffusive regimes, Phys. Rev. B. **79**, 224412 (2009).

[28] G. Woltersdorf, O. Mosendz, B. Heinrich, and C. H. Back, Magnetization Dynamics Due to Pure Spin Currents in Magnetic Double Layers, Phys. Rev. Lett. **99**, 246603 (2007).

[29] G. van der Laan and A. I. Figueroa, X-ray magnetic circular dichroism: A versatile tool to study magnetism, Coord. Chem. Rev. **277**, 95 (2014).

[30] C. J. Durrant, M. Jokubaitis, W. Yu, H. Mohamad, L. R. Shelford, P. S. Keatley, G. Xiao, and R. J. Hicken, Ferromagnetic resonance of patterned chromium dioxide thin films grown by selective area chemical vapour deposition, J. Appl. Phys. **117**, 17B707 (2015).

[31] R. Urban, G. Woltersdorf, and B. Heinrich, Gilbert Damping in Single and Multilayer Ultrathin Films: Role of Interfaces in Nonlocal Spin Dynamics, Phys. Rev. Lett. **87**, 217204 (2001).

[32] M. K. Marcham, L. R. Shelford, S. A. Cavill, P. S. Keatley, W. Yu, P. Shafer, A. Neudert, J. R. Childress, J. A. Katine, E. Arenholz, N. D. Telling, G. van der Laan, and R. J. Hicken, Phase-resolved x-ray ferromagnetic resonance measurements of

[33] M. K. Marcham, P. S. Keatley, A. Neudert, R. J. Hicken, S. A. Cavill, L. R. Shelford, G. van der Laan, N. D. Telling, J. R. Childress, J. A. Katine, P. Shafer, and E. Arenholz, Phase-resolved x-ray ferromagnetic resonance measurements in fluorescence yield, J. Appl. Phys. **109**, 07D353 (2011).

[34] B. Heinrich and J. F. Cochran, Ultrathin metallic magnetic films: Magnetic anisotropies and exchange interactions, Adv. Phys. **42**, 523 (1993).

[35] See Supplemental Material at http://link.aps.org/supplemental/10.1103/PhysRevB.96.144421 for vibrating sample magnetometry data and error estimation in x-ray ferromagnetic resonance fitting.

[36] K. Nomura, S. Kikuchi, M. Yasuda, K. Tokumitsu, and Y. Ujihira, Mossbauer study on Fe-Ag and Fe-Ni-Ag superlaminates prepared by repeated rolling and treated by gas nitriding, Hyperfine Interact. **148**, 307 (2003).

[37] J. O'M. Bockris, B. E. Conway, and R. E. White, *Modern Aspects of Electrochemistry* (Springer Science and Business Media, Berlin, 1992).

[38] H. D. Arnold and G. W. Elmen, Permalloy, a new magnetic material of very high permeability, Bell Labs Tech. J. **2**, 101 (1923).

[39] J. M. Shaw, H. T. Nembach, T. J. Silva, and C. T. Boone, Precise determination of the spectroscopic g-factor by use of broadband ferromagnetic resonance spectroscopy, J. Appl. Phys. **114**, 243906 (2013).

[40] H. T. Nembach, T. J. Silva, J. M. Shaw, M. L. Schneider, M. J. Carey, S. Maat, and J. R. Childress, Perpendicular ferromagnetic resonance measurements of damping and Lande g-factor in sputtered $(Co_2Mn)1-xGe$ x thin films, Phys. Rev. B. **84**, 054424 (2011).

[41] Y. Tserkovnyak, A. Brataas, G. E. W. Bauer, and B. I. Halperin, Nonlocal magnetization dynamics in ferromagnetic heterostructures, Rev. Mod. Phys. **77**, 1375 (2005).